

Growth and transport properties of thin Bi films on InP(110)

This content has been downloaded from IOPscience. Please scroll down to see the full text.

1996 Semicond. Sci. Technol. 11 1575

(<http://iopscience.iop.org/0268-1242/11/11S/021>)

View [the table of contents for this issue](#), or go to the [journal homepage](#) for more

Download details:

IP Address: 169.237.74.113

This content was downloaded on 15/01/2014 at 21:15

Please note that [terms and conditions apply](#).

Growth and transport properties of thin Bi films on InP(110)

B G Briner^{†||}, R M Feenstra^{‡||}, T P Chin[§] and J M Woodall[§]

[†] Abt. Oberflächenphysik, Fritz-Haber-Institut, Faradayweg 4–6, 14195 Berlin, Germany

[‡] Department of Physics, Carnegie Mellon University, Pittsburgh, PA 15213, USA

[§] School of Electrical and Computer Engineering, Purdue University, West Lafayette, IN 47907, USA

Abstract. Growth and lateral charge transport properties of thin ($d = 20\text{--}30 \text{ \AA}$) Bi films are investigated with scanning tunnelling microscopy. Bismuth is deposited at $T = 140 \text{ K}$ onto the cleaved (110) surface of an InP-based heterostructure. Growth at low temperature is kinetically limited and leads to strained, metastable overlayers. After annealing to 300 K the Bi surface consists of atomically flat terraces separated by 12 \AA deep holes. We find that prolonged injection of a high lateral current promotes significant changes in surface morphology which are attributed to a strain relaxation process mediated by electromigration. Scanning tunnelling potentiometry is applied to probe the local response of the semimetal overlayers to the injected lateral current. The observed potential distribution provides evidence for both phonon and defect scattering. At the position of holes and grain boundaries we find typically 2–4 mV high potential steps. It is argued that these steps indeed reflect a localized increase of the film resistance and cannot be attributed to tip-convolution artefacts.

1. Introduction

The scanning tunnelling microscope (STM) has evolved into a powerful and flexible experimental tool which provides insights into a broad variety of atomic-scale processes on metal and semiconductor surfaces [1]. STM-based experiments aimed at investigating charge transport in low-dimensional structures fall into two different categories. Studies on *perpendicular* transport across small barriers, clusters or constrictions use the tunnelling current as the source for the transport process. The excellent spatial confinement of the tunnelling current makes it possible to probe structures down to the atomic scale. Information on the specific interactions which characterize the transport process is reflected in the dependence of the conductivity across the nanostructure on the applied bias voltage. Examples for such experiments are the observation of single-electron tunnelling in double barrier structures [2], and the investigation of quantized conduction across small wires pulled with the STM tip [3]. Thanks to the small size of the investigated structures both studies succeed in finding evidence of quantum transport even at room temperature. In addition, the project on quantum wires nicely demonstrates how the STM can be employed to both fabricate and probe a nanostructure.

^{||} Experiments performed at: IBM, T J Watson Research Center, Yorktown Heights, NY 10598, USA

The second group of transport-related experiments with an STM concentrates on *lateral* transport in planar structures. Here the source current for the sample under investigation is supplied via external contacts while the STM tip probes the local electrochemical surface potential with almost atomic lateral resolution. This scanning tunnelling potentiometry (STP) technique was introduced by Murali and Pohl to study charging effects in granular Au films [4]. The same authors applied STP for cross-sectional imaging of a GaAs/AlGaAs heterostructure, and illustrated how the shape of the depletion regions depends on the lateral bias voltage [5]. Kirtley *et al* improved the sensitivity of STP to the 10 μV level, and reported the observation of potential steps at grain boundaries of 600 \AA thick granular Au₆₀Pd₄₀ films [6]. These discontinuities in the potential were ascribed to strong scattering at the grain boundaries, in line with a long-standing theory by Landauer [7] which predicts that localized scatterers give rise to local current and field variations. A subsequent study [8] seriously questioned the interpretation of Kirtley *et al*, and argued that potential steps in STP images can appear as artefacts caused by convolution of the STM tip with the substantial corrugation of the investigated surface. Such tip-convolution effects get larger on a rough sample surface, and they also increase in size for a blunt probe tip. This behaviour is opposite to the intuitive expectation based on topographic imaging where a poor-quality tip produces blurred and featureless results.

Several groups have tried to further improve the detection sensitivity of STP [9–11] with the motivation of finding evidence for defect scattering on flat parts of the metal film where tip-convolution artefacts can be excluded. Instead of further optimizing the detection technique we have taken an alternative approach to tunnelling potentiometry which is based on a novel sample geometry and has made it possible to unambiguously observe scattering-induced discontinuities in the surface potential of thin Bi films [12]. Here we describe these experiments in detail with particular emphasis on the growth of the semimetal films and on the observation of potential steps at grain boundaries.

2. Experimental details

For the present experiments our goal has been to optimize the sample geometry in order to overcome the limitations imposed on STP by a rough surface. On the insulating substrates (quartz, mica) which were used in earlier potentiometry studies metal growth usually proceeds via island formation. To obtain continuous films requires the deposition of several hundred angstroms thick layers with obvious consequences for the surface corrugation. In contrast, it has been demonstrated that it is possible to grow continuous and flat semimetal (Bi, Sb) films on the cleaved (110) surface of GaAs and InP [13–16]. To benefit from these favourable growth conditions we have developed a substrate which consists of an n–i–n heterostructure on top of an InP wafer. The heterostructure is used to inject a high lateral current into a narrow segment of an evaporated semimetal film. Figure 1 shows a schematic layout of this heterostructure together with a functional diagram of the STP set-up. The choice of degenerately n-doped $\text{In}_{0.53}\text{Ga}_{0.47}\text{As}$ for the contact layers is dictated by the need to avoid the formation of Schottky barriers at the interfaces to the evaporated conductor which would inhibit efficient current injection. For a dopant concentration of $n = 10^{19} \text{ cm}^{-3}$ the Fermi level of $\text{In}_{0.53}\text{Ga}_{0.47}\text{As}$ is significantly shifted into the conduction band, and it can be expected to form ohmic contacts to the metal overlayer. The 5000 Å thick spacer layer consists of either semi-insulating, Fe-doped InP or low-temperature MBE-grown, slightly p-doped $\text{In}_{0.52}\text{Al}_{0.48}\text{As}$. This spacer is separated from the outer contact layers by two 1000 Å thick, moderately n-doped $\text{In}_{0.53}\text{Ga}_{0.47}\text{As}$ buffers. We have found that, in particular for the substrates with $\text{In}_{0.52}\text{Al}_{0.48}\text{As}$ spacer layers, these buffers are necessary to avoid interband tunnelling which would result in a low shunt resistance. To provide electrical contacts to the substrate holder, gold films are evaporated onto the topmost layer of the heterostructure and onto the back side of the InP-wafer. The top contact is left unannealed, because diffusion of Au into the heterostructure would create shunts across the insulating spacer.

To prepare a flat semimetal overlayer we start by cleaving the samples in the same ultra-high vacuum (UHV) system which is used for the STP experiments. Immediately after cleavage, the substrates are cooled down to $T = 140 \text{ K}$ and bismuth is evaporated onto the cleaved edge. Before resorting to this low-temperature deposition technique we

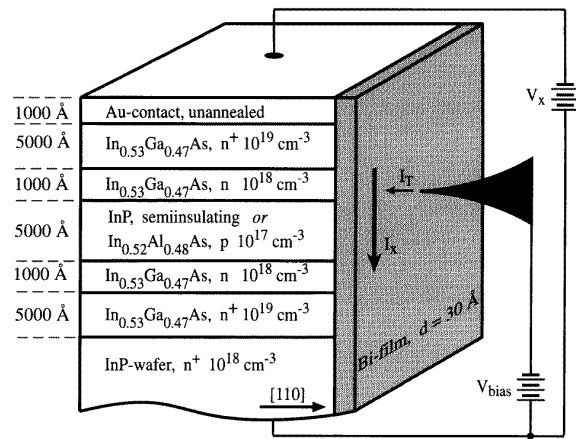


Figure 1. The sample geometry. Bi is deposited onto the cleaved edge of an n–i–n heterostructure. The potential drop on the portion of the Bi film bridging the i layer is probed with the STM.

have investigated the room temperature growth of Bi and Sb. Unfortunately, for both materials it was impossible to obtain flat films at $T = 300 \text{ K}$. During Bi evaporation the sample resistance is continuously monitored to check for the formation of a conducting bridge across the i layer. For deposition at 140 K the resistance starts to drop at a threshold of only 6 Å. This is a clear indication for the flat and continuous growth of the Bi films. Analogous experiments were performed at different temperatures and with Sb and Be as alternative evaporation materials. We found that for these materials a much thicker layer ($>50 \text{ Å}$) had to be deposited before the sample resistance started to decrease. It should be emphasized that due to imperfections in the i layer the percolation limit cannot be properly detected, since at this point the overlayer still has a much poorer conductance than the substrate. Nevertheless, STM topographs indicate a clear correspondence between a rough surface morphology and a large percolation threshold during growth. Because all STP experiments are performed at room temperature we have to anneal the Bi films to 300 K after low-temperature deposition. We find that the thinnest Bi films become discontinuous upon heating to 300 K. Therefore we are presently restricted to the investigation of films with a thickness of at least 15–20 Å. All layer thicknesses quoted in this study are derived from the readings of a crystal deposition monitor i.e. they should be understood as average values.

Topographic and potentiometric data on these Bi films are obtained with a UHV STM equipped with facilities for *in situ* tip and sample change [17]. Single-crystal W tips are cleaned by sputtering and heating until they show a sharp and stable field-emission pattern. STM topographs are recorded with a constant tunnelling current of 100 pA and a sample bias of the order of 100 mV. For the potentiometry experiments we disable the STM feedback loop at each image pixel, and record a current–voltage (I – V) curve which typically extends over an interval of $\pm 50 \text{ mV}$ around the local electrochemical potential V_0 on the surface. The tip–surface distance is intentionally

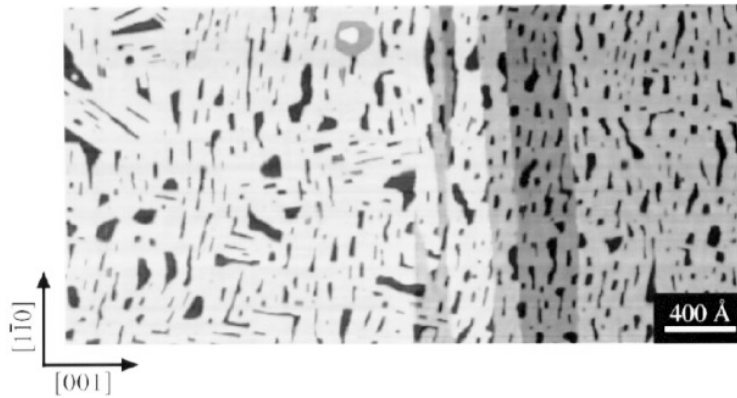


Figure 2. Topography image of a 20 Å thick Bi film grown at $T = 140$ K on InP(110). $V_{bias} = 250$ mV, $I_T = 100$ pA, field of view: $3900 \text{ \AA} \times 1950 \text{ \AA}$.

reduced by 1 Å after disabling the feedback loop in order to increase the current-detection sensitivity close to the zero-crossing point. After the experiment, the measured $I-V$ data are interpolated with third-order polynomials, and an STP image is generated from the zeros of these fit curves which represent the experimental approximation for V_0 . We find that in our set-up the detection sensitivity is currently limited to 0.5 mV by external noise sources. The spectroscopic data confirm that all investigated Bi films are good conductors because their $I-V$ curves are almost linear close to V_0 .

3. Results and discussion

3.1. Growth of Bi on InP(110)

The investigation of 20–30 Å thick Bi films using an STM shows that under the described growth conditions bismuth forms continuous overlayers which are characterized by atomically flat planes interspersed with irregularly shaped holes. The typical surface morphology found in the present study is illustrated in figure 2, a large-scale STM topograph recorded on a nominally 20 Å thick Bi layer. Many small, always 12 Å deep, holes are discernible. This large step height corresponds to the size of the pseudocubic unit cell of Bi in the (111) direction. The formation of such large steps is somewhat unexpected. Structural studies of thicker Bi layers deposited at room temperature on GaAs [15] and InP [14] found that the surface usually consists of terraces separated by 4 Å high steps. We attribute the morphology of our films to the growth at low temperature which is kinetically limited and consequently leads to strained and metastable overlayers. Patrín *et al* [16] have reported a similar influence of the deposition temperature on the surface structure of Bi films grown on GaAs and InP, but they find smaller (7 Å) steps, probably due to different film thicknesses and growth conditions. The elongated vertical steps visible in figure 2 are cleavage defects on the heterostructure which are replicated in the semimetal overlayer. As will be shown below, this particular growth mode of Bi is a favourable prerequisite for the potentiometry experiments because apart from the holes the film surface is flat on a scale of several 1000 Å.

The hypothesis that after growth the films are in a metastable state is confirmed by the observation that injecting a high lateral current for a prolonged time induces significant changes in surface morphology. Figure 3 shows a $7900 \text{ \AA} \times 4800 \text{ \AA}$ topography image ($d_{Bi} = 20 \text{ \AA}$) recorded on the part of the Bi film over the heterostructure which is exposed to the lateral current. Before taking this image, an average current density of $3.5 \times 10^6 \text{ A cm}^{-2}$ has been run through the film for 8 h. Near the right border of figure 3 the ‘as-grown’ structure is still visible. However, most of the film surface has drastically changed. The 12 Å deep holes have been replaced by large terraces separated by 4 and 8 Å high steps. In the strained phase, the surface defects are preferentially aligned along the (110) direction of the substrate, a fact which underlines that this growth mode is strongly influenced by the misfit between substrate and overlayer lattices. In contrast, the islands in the relaxed phase are more isotropic in shape, and the step orientations reflect the approximately hexagonal symmetry of the Bi surface. Occasionally, deep holes appear also in this relaxed phase. Such holes present both an opportunity and a technical problem for the potentiometry experiments. On one hand, the deep holes constitute dominant scattering centres for the lateral current which allow for a detailed study of the transport-induced potential distribution. On the other hand, the steep steps and the reduced conductivity inside the holes make scanning across such defects difficult and prone to tip-crashes.

It may be argued that the observed changes in surface morphology are caused by locally heating the Bi film with the applied current. To test whether the strain relaxation process is thermally stimulated we have annealed the sample on which figure 3 was recorded to $T = 420$ K for 30 min. By imaging a part of the semimetal film which has *not* been subjected to a lateral current we can make sure that here any observed deviations from the ‘as-grown’ phase must be thermally induced. Figure 4 shows that the surface morphology has also changed in response to thermal annealing, but the resulting structure is significantly different compared to the current-induced effects. The slightly elongated, 12 Å deep holes are still present and the average lateral size of these defects has significantly increased. Periodic fringes (corrugation

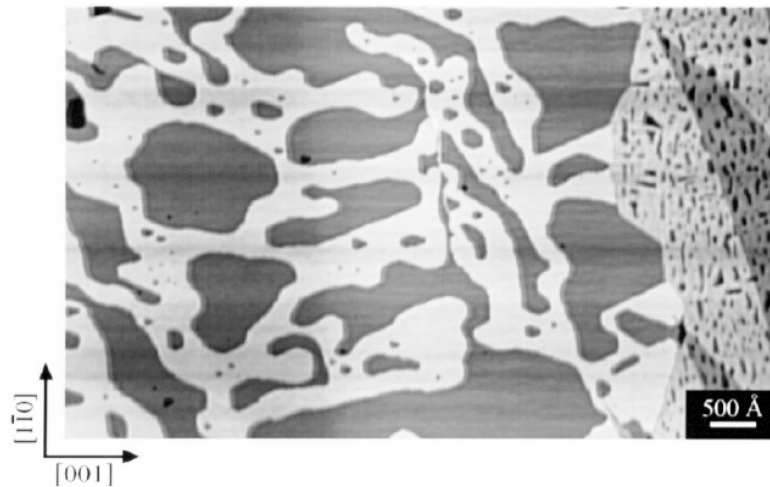


Figure 3. STM topograph ($7900 \text{ \AA} \times 4800 \text{ \AA}$) showing the change of surface morphology in response to lateral current injection. $d_{\text{Bi}} = 20 \text{ \AA}$. The strained phase (still visible near the right border of the image) transforms into large terraces with step heights of 4 and 8 Å.

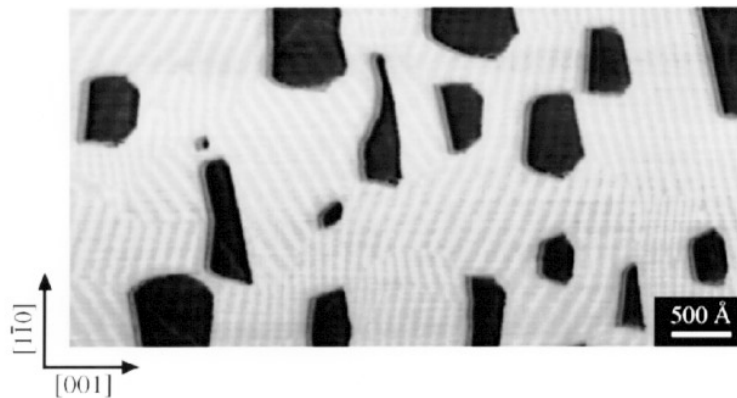


Figure 4. Same film as in figure 3 after annealing to $T = 420 \text{ K}$. Topography image of a part of the Bi film on the InP wafer which has not been subjected to a lateral current. Field of view: $5600 \text{ \AA} \times 2800 \text{ \AA}$.

amplitude $\sim 1 \text{ \AA}$) now appear on the flat parts of the surface. These fringes are similar to the moiré pattern which has been reported by Patrin *et al* [16], and which was explained as a result of the misfit between substrate and overlayer lattice constants. The varying angle of the fringes with respect to the substrate nicely illustrates the existence of differently oriented domains in these polycrystalline films. The observation that domain boundaries often originate from the surface defects lets us suggest that the holes act as pinning centres for the metastable surface. We observe similar fringes with a much reduced corrugation amplitude also on thin ($d = 20 \text{ \AA}$) Bi films in the ‘as-grown’ phase. Based on the significant difference between figures 3 and 4 we propose that strain relaxation on the part of the film over the heterostructure is promoted by electromigration in response to the high injected lateral current. This interpretation is confirmed by a numerical estimate of Ohmic heating. Assuming intimate contact between film and substrate, we find that a lateral current density of $5 \times 10^6 \text{ A cm}^{-2}$ leads to a temperature rise of less than 1 K. Electromigration alone cannot be made responsible for the current-induced structural changes. It leads to an oriented

motion of atoms along the direction of the current [18], but the surface structure shown in figure 3 does not provide evidence for such an oriented mass flow. Therefore, we tentatively suggest that electromigration sets in at the 12 \AA holes where the local electric field is enhanced (see below). By selectively reshaping and removing the pinning centres, electromigration lowers the potential barrier for thermally assisted strain relaxation which finally transforms the surface into the observed isotropic structure.

3.2. Potentiometry

Potentiometry experiments are carried out on 20–30 Å thick Bi films subjected to current densities of the order of 10^6 A cm^{-2} . They always reveal the coexistence of both phonon and defect scattering in the investigated films. Figure 5 presents simultaneously recorded topography (a) and potential images (b) on a 30 Å thick Bi film. The potential image covers a greyscale range of 34 mV. A horizontal potential ramp is clearly visible. It corresponds to the resistance caused by electron–phonon scattering in a film with constant thickness, and obviously represents

a significant portion of the total film resistance at room temperature. However, in addition to the ramp we find small steps in the surface potential coinciding with the positions of the defects on the topography image. To better illustrate the formation of these typically 2–4 mV high steps, figure 5(c) presents line-cuts of the potential distribution along the direction of the externally applied field. The two holes which cause the depicted potential steps have a horizontal extension a of 30 and 50 Å. The topographic information on the defect size and the measured potential ramp which, for this image, corresponds to a field of $E_x = 31 \mu\text{V} \text{ \AA}^{-1}$ allow us to determine an upper bound for the possible influence of tip-convolution artefacts on the shape of the line-plots shown in figure 5(c). Assuming that *no* voltage drop occurs at the holes, the distortion of the uniform ramp by tip convolution could at most lead to voltage steps of $\Delta V = E_x a$. As indicated in figure 5(c) these steps are significantly smaller than the observed discontinuities. In contrast to tip convolution which only locally distorts the potential ramp, the steps in the experimental data lead to an offset between the flat parts of the potential curve i.e. they represent a real resistance increase. It must be emphasized that an almost perfect film surface is an important prerequisite for interpreting the potentiometry data. The simple linear background ramp which makes it possible to easily separate phonon and defect scattering is a direct consequence of the fact that apart from the holes the films are atomically flat.

A network of faint lines connecting the surface defects is visible in figure 5(a). These lines are grain boundaries which separate differently oriented crystallites of the Bi film. The potential distribution near a vertical grain boundary has been highlighted in figure 5(b) by locally changing the greyscale repartition. A small step corresponding to $\Delta V_0 < 1$ mV is visible. It must be pointed out that such small potential features are close to the detection limit of our STP set-up which is currently restricted to ~ 0.5 mV by external noise sources. We find that for the thinnest studied Bi films the grain boundaries give rise to more pronounced potential discontinuities. A larger misfit-induced strain in these films probably leads to an increased scattering cross-section at the grain boundaries. Figure 6 presents topography and STP images which have been recorded on a 20 Å thick Bi film subjected to a lateral current density of $1.5 \times 10^6 \text{ A cm}^{-2}$. Grain boundaries appear as bright lines in the STM-topograph (a). Due to a somewhat blunt probe-tip the borders of the 12 Å deep holes appear blurred. The potential image (b) displays similar features to those visible in figure 5. However, here the highlighted portion of the image clearly shows the formation of a potential step at the grain boundary. For this film not only the domain boundaries but also the fringe pattern, which has been discussed in the preceding section, can be discerned in both the topography and potential images. This finding illustrates the existence of localized scattering at defects down to the atomic scale.

A rough sample surface does not only increase the chance for tip-convolution, it also makes it difficult to distinguish between artefacts and real potential discontinuities. The background contribution to the

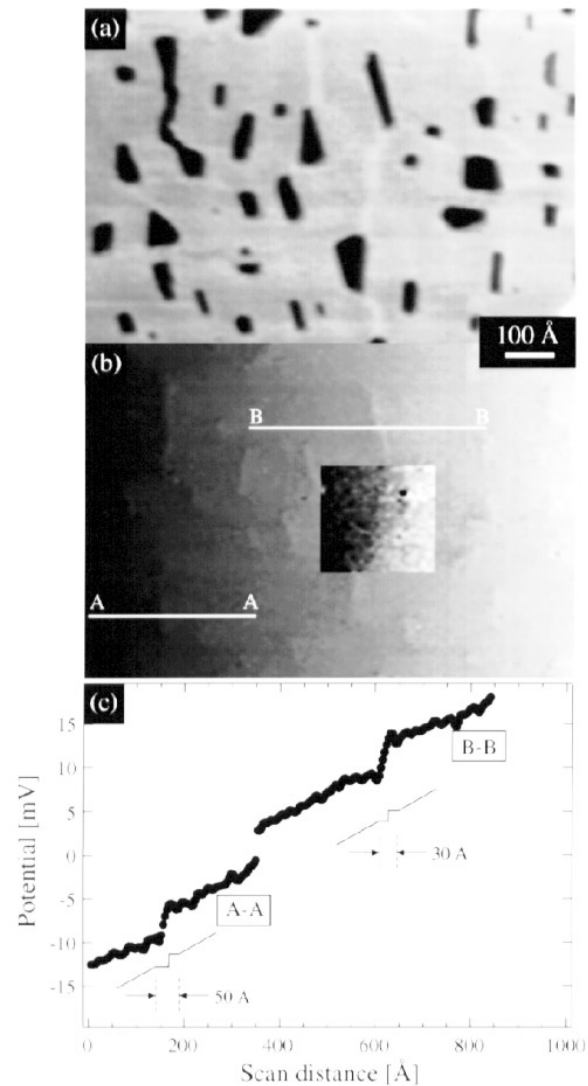


Figure 5. (a) An STM topograph. (b) A simultaneously recorded STP image on a 30 Å thick Bi film. Potential discontinuity at grain boundary is highlighted. (c) This graph presents line-cuts across the potential image as marked in (b) and shows the expected potential slopes if the steps were entirely caused by tip convolution.

resistance of a rough film changes on a small scale, and consequently no smooth potential ramp can be observed by STP. As explained in section 2, the surface quality of the Bi films strongly depends on the deposition temperature. Figure 7(a) shows the surface of a nominally 25 Å thick Bi film which has been prepared by evaporation at a somewhat higher temperature ($T \approx 200$ K). The enhanced atomic mobility during deposition obviously has led to the formation of a granular surface structure. On the potential image in figure 7(b) a ramp is still discernible, but the potential distribution is dominated by strong discontinuities which are suggestive of transport across an almost disconnected layer. It is possible that some of these discontinuities appear artificially enhanced. However, tip-convolution cannot be made responsible for the inverted potential steps marked by arrows in figure 7(b). Such a

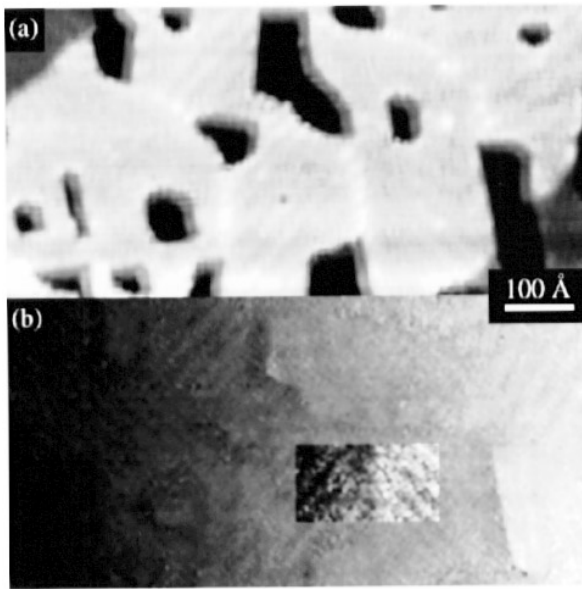


Figure 6. Topography (a) and potential images (b) on a 20 Å thick Bi film. Lateral current density = 1.5×10^6 A cm⁻². A potential step at a grain boundary has been highlighted in (b) by locally changing the greyscale repartition.

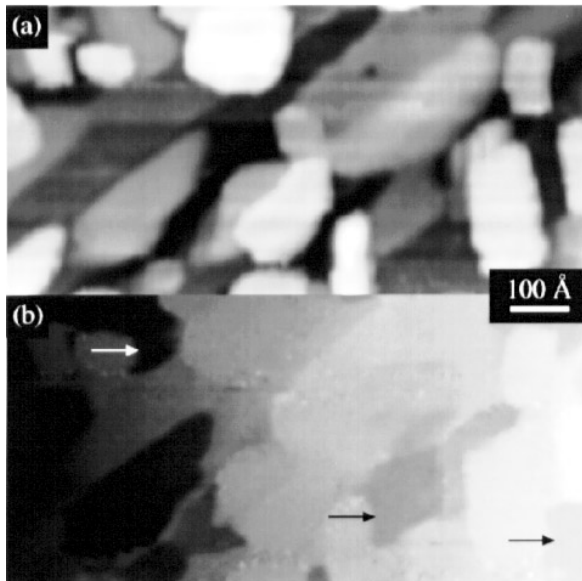


Figure 7. (a) A nominally 25 Å thick Bi film. Growth at $T = 200$ K results in a rough surface. (b) The corresponding potential image is characteristic for an almost disconnected film. Inverted potential steps are marked by arrows.

field inversion indicates either a local current flow opposed to the direction of the applied field or the prevalence of charging effects.

The deep holes which appear on the semimetal films as a result of the described strain relaxation process act as strong scatterers. We have found [12] that they give rise to very pronounced potential discontinuities (step size >20 mV). In the vicinity of a hole, the ‘net’ potential

after subtraction of a linear background takes on the shape of a two-dimensional dipole. The lobes of the dipole extend over several hundred angstroms beyond the geometric size of the defect. The observation of deviations from the background ramp on *flat* parts of the surface makes it possible to unambiguously assign the dipole to defect scattering even though tip-convolution artefacts *within* the deep holes cannot be excluded. The fact that the observed potential resembles the theoretically predicted resistivity dipole [7, 19] motivates the question about the relative importance of ballistic (electron–electron) and diffusive (electron–phonon) scattering which is discussed in detail in [12]. We find that in the present room-temperature experiments diffusive scattering makes the main contribution to the observed potential discontinuities, but ballistic effects are also identified. From the low carrier density in bulk Bi one would expect that ballistic transport dominates even at room temperature. However, this apparent contradiction is resolved by noting that surface states can significantly increase the effective carrier concentration in thin Bi films [20].

In summary, the presented results provide clear evidence for defect scattering at room temperature i.e. the potential discontinuities represent a direct fingerprint of residual resistivity. The novel sample geometry could also make it possible to observe some of the finer details in the scattering-induced potential distribution, such as the predicted Friedel oscillations [19, 21], if a similar experiment is performed at low temperature.

Acknowledgments

We would like to thank R Landauer and J Kirtley for helpful discussions. One of us (BB) gratefully acknowledges financial support by the Schweizerischer Nationalfonds.

References

- [1] Güntherodt H-J and Wiesendanger R (eds) 1994 *Scanning tunnelling Microscopy I (Springer Series Surface Science 20)* 2nd edn (Berlin: Springer)
- [2] Schönenberger C, van Houten H and Donkersloot H C 1992 *Europhys. Lett.* **20** 249
- [3] Olesen L, Lægsgaard E, Stensgaard I, Besenbacher F, Schiøtz J, Stoltze P, Jacobsen K W and Nørskov J K 1994 *Phys. Rev. Lett.* **72** 2251
Brandbyge M, Schiøtz J, Sørensen M, Stoltze P, Jacobsen K W, Nørskov J K, Olesen L, Lægsgaard E, Stensgaard I and Besenbacher F 1995 *Phys. Rev. B* **52** 8499
- [4] Muralt P and Pohl D 1986 *Appl. Phys. Lett.* **48** 514
- [5] Muralt P, Meier H, Pohl D W and Salemink H W M 1987 *Appl. Phys. Lett.* **50** 1352
- [6] Kirtley J R, Washburn S and Brady M J 1988 *Phys. Rev. Lett.* **60** 1546
- [7] Landauer R 1957 *IBM J. Res. Dev.* **1** 223
Landauer R 1975 *Z. Phys. B* **21** 247
- [8] Pelz J P and Koch R H 1990 *Phys. Rev. B* **41** 1212
- [9] Besold J, Reiss G and Hoffmann H 1993 *Appl. Surf. Sci.* **65/66** 23
- [10] Möller R, Baur C, Esslinger A and Kürz P 1991 *J. Vac. Sci. Technol. B* **9** 609
- [11] Koslowski B and Baur C 1995 *J. Appl. Phys.* **77** 28

- [12] Briner B G, Feenstra R M, Chin T P and Woodall J M 1996 *Phys. Rev. B* **54** R5283
- [13] Annovi G, Betti M G, del Pennino U and Mariani C 1990 *Phys. Rev. B* **41** 11 978
- [14] Resch U, Esser N and Richter W 1991 *Surf. Sci.* **251/252** 621
- [15] Patrin J C, Li Y Z, Chander M and Weaver J H 1992 *Phys. Rev. B* **46** 10 221
- [16] Patrin J C, Li Y Z, Chander M and Weaver J H 1993 *J. Vac. Sci. Technol. A* **11** 2073
- [17] Feenstra R M 1994 *Phys. Rev. B* **50** 4561
- [18] See e.g. Landauer R and Woo J W F 1974 *Phys. Rev. B* **10** 1266
Sham L J 1975 *Phys. Rev. B* **12** 3142
- Sorbello R S and Dasgupta B 1977 *Phys. Rev. B* **16** 5193
The relative influence of local electric field (direct force) and momentum exchange with the moving charges (electron wind force) on the mass transport is still debated.
- [19] Zwerger W, Bönig L and Schönhammer K 1991 *Phys. Rev. B* **41** 6434
- [20] Hoffman C A, Meyer J R, Bartoli F J, Di Venere A, Yi X J, Hou C L, Wang H C, Ketterson J B and Wong G K 1993 *Phys. Rev. B* **48** 11 431
Komnik Yu F, Bukhstab E I, Nikitin Yu V and Andrievskii V V 1971 *Sov. Phys.-JETP* **33** 364
- [21] Sorbello R S 1981 *Phys. Rev. B* **23** 5119